Volume 28
Number 20
27 May 2026
Pages 12101–12664

PCCP

Physical Chemistry Chemical Physics

rsc.li/pccp

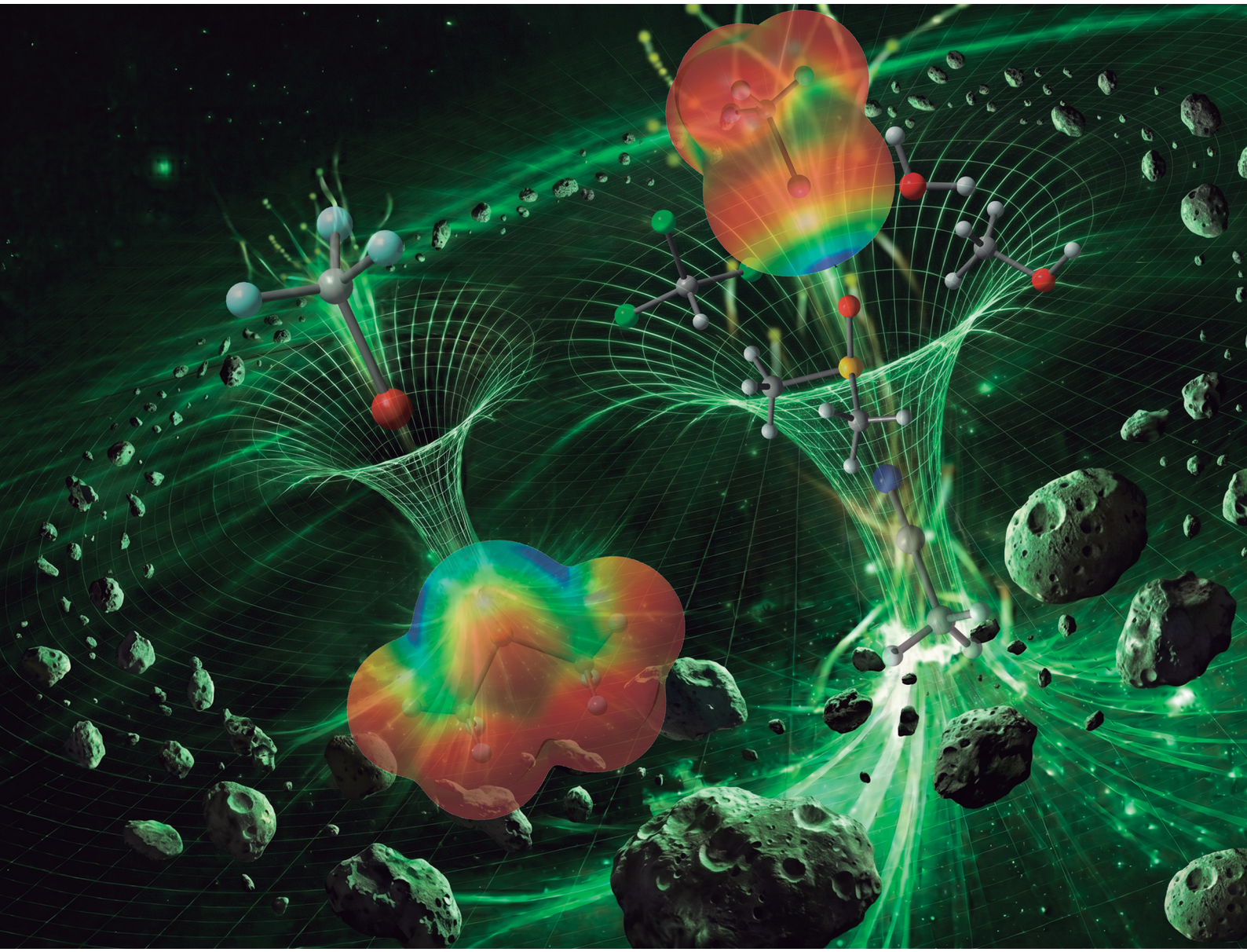

ISSN 1463-9076

ROYAL SOCIETY OF CHEMISTRY

PAPER

Antonio Frontera *et al.*

Evaluation of the solvent competitive binding in halogen and chalcogen bonding: a theoretical theory study for supramolecular applications

PCCP Owner Societies

PCCP

ROYAL SOCIETY OF CHEMISTRY

PAPER

View Article Online
View Journal | View Issue

Cite this: *Phys. Chem. Chem. Phys.*, 2026, **28**, 12188

Evaluation of the solvent competitive binding in halogen and chalcogen bonding: a theoretical theory study for supramolecular applications

Eric Miguens,[a] Mariana Rocha[b] and Antonio Frontera *[a]

Received 6th April 2026,
Accepted 7th May 2026

DOI: 10.1039/d6cp01283c

rsc.li/pccp

Noncovalent interactions such as halogen bonding (HaB) and chalcogen bonding (ChB) are increasingly utilized in host–guest chemistry and supramolecular catalysis due to their high directionality and tuneable strength. However, the choice of solvent remains a critical challenge, as solvent molecules can compete with the intended substrates for the electrophilic σ-hole sites of the catalysts or receptors. In this work, we present a comprehensive DFT study (PBE0-D3/def2-TZVP) analysing the competitive binding of nine common solvents (acetonitrile, ether, water, methanol, DMF, DMSO, dichloromethane, chloroform and acetone) with four model electrophilic probes: CF_3–I, CF_3–Br, CF_3–Se–CF_3, and CF_3–Te–CF_3. By evaluating the interaction energies and Molecular Electrostatic Potential (MEP) surfaces, accounting for the dielectric constant of each medium, we establish a classification of solvent competitiveness. Our results provide an experimental guide for identifying the least competitive solvents, thereby optimizing the efficiency of HaB and ChB driven molecular recognition and catalytic processes in solution.

Introduction

Noncovalent interactions serve as the fundamental ''glue'' of supramolecular chemistry, governing the self-assembly of complex architectures and the specific recognition between hosts and guests.[1] Unlike covalent bonds, these forces are typically characterized by lower bond energies and reversible nature, allowing for dynamic and stimuli-responsive systems.[2–7] The precise control of these interactions has enabled the development of sophisticated functional materials,[8] synthetic receptors,[9] and enzyme-mimetic catalysts.[10] As the field moves toward increasingly complex environments,[11–15] understanding the subtle balance of these forces, especially in the presence of competing species, becomes paramount for the rational design of supramolecular assemblies.[16–25]

A key advancement in the description of noncovalent forces is the σ-hole model.[26,27] A σ-hole is a region of positive electrostatic potential located on the extension of a covalent bond to an electronegative or polarizable atom.[28,29] This electron-deficient region allows the atom to act as an electrophile, attracting Lewis bases and nucleophiles.[30,31] The strength and size of the σ-hole are influenced by the polarizability of the atom and the electron-withdrawing capacity of the attached substituents.[32,33] These σ-hole interactions are remarkably directional, a feature that distinguishes them from more isotropic forces like ion-dipole interactions, making them ideal for the construction of highly organized molecular frameworks.[34–36]

Among σ-hole interactions, halogen bonding (HaB)[37,38] and chalcogen bonding (ChB)[39,40] have emerged as powerful tools for molecular recognition and organocatalysis.[41] As highlighted in recent literature, HaB (involving Group 17 elements) and ChB (involving Group 16 elements like Se and Te) offer unique advantages in solution-state chemistry, such as high water tolerance in specific cases and the ability to operate in hydrophobic pockets of proteins.[42–50] These interactions are now frequently employed to stabilize transition states in synthetic transformations or to create selective sensors for anions and neutral molecules.[51–61] However, the effectiveness of a HaB or ChB donor in solution is often hampered by the solvent itself.[62] Because many common organic solvents possess lone pairs (*e.g.*, on O, N, or S atoms), they can act as Lewis bases and occupy the σ-hole of the donor, effectively ''poisoning'' the catalyst or blocking the receptor site.

The purpose of the present manuscript is to provide a systematic classification of common laboratory solvents based on their competitiveness for σ-hole sites. To achieve this, we have performed a detailed DFT study at the PBE0-D3/def2-TZVP level of theory, examining the interaction of acetonitrile, ether, water, methanol, DMF, DMSO, dichloromethane, chloroform and acetone with four representative model molecules: CF_3I, CF_3Br, $(CF_3)_2Se$, and $(CF_3)_2Te$ (see Scheme 1). By incorporating

[a] *Departament de Química, Universitat de les Illes Balears, Crta de Valldemossa km 7.5, 07122, Palma de Mallorca, Baleares, Spain. E-mail: toni.frontera@uib.es*
[b] *INBIOFAL (CONICET – UNT), Instituto de Química Orgánica, Facultad de Bioquímica, Química y Farmacia, Universidad Nacional de Tucumán, Ayacucho 471, San Miguel de Tucumán, Argentina*

solvents	abbreviations	ε
H_2O	W	80.4
CH_3SOCH_3	DMSO	46.7
CH_3CN	ACN	37.5
$HCON(CH_3)_2$	DMF	37.7
CH_3OH	MeOH	32.6
CH_3COCH_3	ACE	20.7
CH_2Cl_2	DCM	9.0
$CHCl_3$	TCM	4.8
Et_2O	DEE	4.3

σ-hole donors:

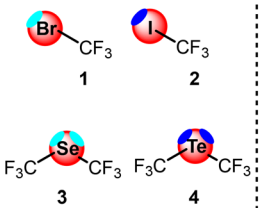

Scheme 1 Solvents, abbreviations used in this work, dielectric constants and σ-hole donor molecules.

the dielectric constant of each solvent into our MEP and energy calculations, we simulate realistic solution-phase conditions. This study aims to identify the "least competitive" solvents for each class of interaction, offering a practical hierarchy to assist experimentalists in selecting the optimal media for supramolecular catalysis and host–guest chemistry.

Theoretical methods

All electronic structure calculations were performed using the Gaussian 16 software package.[63] The geometries of the four model molecules (CF_3I, CF_3Br, $(CF_3)_2Se$, and $(CF_3)_2Te$), the seven solvent molecules, and their corresponding binary complexes were fully optimized without any symmetry constraints. The PBE0 hybrid functional[64] was employed in combination with the Grimme's D3 dispersion correction[65] to accurately account for long-range dispersion effects, which are critical in describing noncovalent interactions. The def2-TZVP basis set[66] was utilized for all atoms to ensure a high-quality description of the electronic density and the polarizability of the heavier halogen and chalcogen atoms.

To simulate the influence of the chemical environment on the interaction strength and electronic properties, the Polarizable Continuum Model (PCM) was used.[67] Specifically, the dielectric constant (ε) corresponding to each of the seven solvents was incorporated into the calculations for the respective systems. The interaction energies were calculated as the difference between the energy of the complex and the sum of the energies of the isolated monomers, both optimized in the corresponding dielectric medium.

While Gibbs free energies (ΔG) were calculated to assess the thermodynamic stability of the complexes, the discussion in this work focuses primarily on the interaction energies (ΔE) corrected for solvent effects. This approach was chosen because standard gas-phase entropic corrections often overestimates the dissociative character of these complexes in a condensed phase, where the high concentration of solvent molecules favors occupancy of the electrophilic sites. By focusing on ΔE, we provide a direct comparison of the electronic competitiveness of the solvent lone pairs for the σ-hole, independent of the large entropic penalties associated with bimolecular association in a continuum model. For completeness, the calculated ΔG values for all studied complexes are provided in the SI (Table S1).

The molecular electrostatic potential (MEP) surfaces were computed at the same level of theory to identify and quantify the electrophilic σ-holes on the iodine, bromine, selenium, and tellurium atoms and the nucleophilic σ-lumps at the solvent molecules. These MEP analyses also accounted for the specific dielectric constant of the medium to evaluate how solvent polarity modulates the electrostatic landscape of the donors. The resulting MEP maps and potential extrema ($V_{s,max}$) were visualized and plotted using the GaussView 6.0 interface.

Finally, the topological properties of the electron density were analyzed through the Atoms in Molecules (AIM) theory[68] using the AIMAll program.[69] This analysis was performed to confirm the existence of the noncovalent bonds and to characterize the nature of the HaB and ChB interactions *via* the identification of bond critical points (BCPs) and the evaluation of the electron density (ρ) at these points.

Results and discussion

MEP analysis

The MEP values at the σ-hole of compounds **1–4**, calculated using the dielectric constant of the different solvents, are summarized in Table 1, with corresponding plots shown in Fig. 1. The results indicate that the use of a continuum model for the solvent has a minimal influence on the σ-hole potential, as only small differences are observed across the various media. As expected, the σ-hole values are more positive for the heavier elements, specifically tellurium and iodine. Furthermore, the MEP values reveal that tellurium in compound **4** is more electrophilic than iodine in compound **2**. This increased electrophilicity is likely due to the presence of two electron-withdrawing trifluoromethyl substituents in compound **4** compared to the single substituent in the halogenated model.

To further characterize the nature of these electrophilic regions, we examined the variation of the MEP as a function of the angle α (see Fig. 2). For the halogen bond donors **1** and **2** (Fig. 2a), α = 0° corresponds to the location of the σ-hole, while α = 90° represents the location of the negative belt. Interestingly, in the case of bromine (**1**), the MEP drops significantly when moving only 15° away from the σ-hole, and at 45°, the potential is close to 0°. In contrast, for iodine (**2**), the MEP

Table 1 MEP values ($V_{s,max}$) at the σ-holes of compounds **1–4** in different solvents

Medium	1	2	3	4
Water	24.9	34.2	26.8	37.6
DMSO	24.8	34.2	26.7	37.5
Acetonitrile	24.8	34.1	26.7	37.5
DMF	24.8	34.1	26.7	37.5
Methanol	24.8	34.1	26.7	37.4
Acetone	24.8	34.0	26.6	37.3
Dichloromethane	24.6	33.6	26.3	36.8
Trichloromethane	24.4	33.2	25.9	36.0
Diethylether	24.3	33.1	25.7	35.8

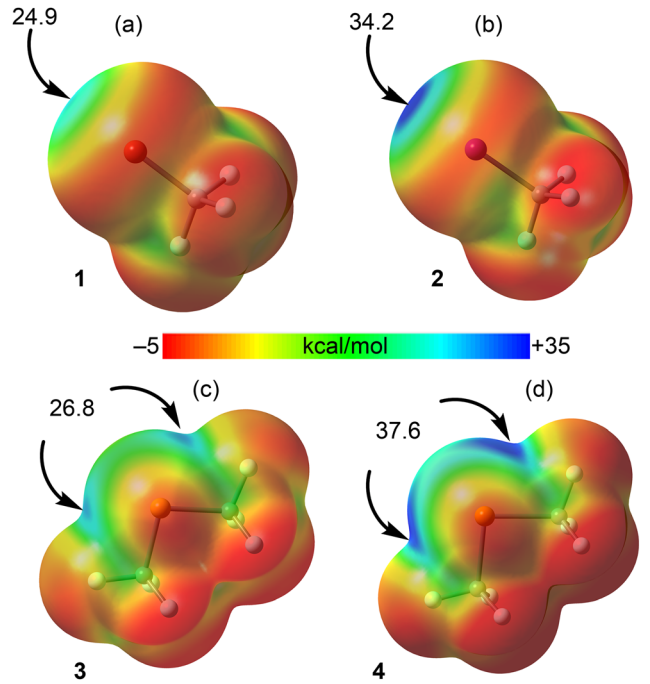

Fig. 1 MEP surfaces of compounds **1** (a), **2** (b) **3** (c) and **4** (d) using a continuum model of water. Isovalue 0.001 a.u.

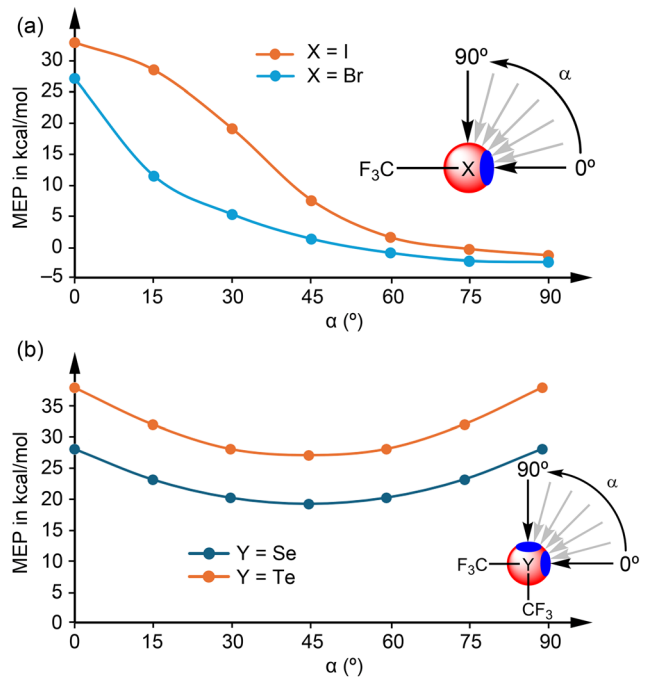

Fig. 2 Variation of the MEP (kcal mol^{-1}) as a function of the angle alpha (α) for halogen bond donors **1** and **2** (a) and chalcogen bond donors **3** and **4** (b). In (a), α = 0° corresponds to the σ-hole axis and α = 90° to the negative belt. In (b), the angle α scans the molecular plane between the two symmetric σ-holes. All values were calculated in a continuum model of water.

diminishes more slowly, showing only a small variation at 15°. This suggests a higher degree of directionality for the halogen bond involving bromine compared to iodine.

Table 2 MEP values ($V_{s,min}$) at the lone pairs of the solvents using its own dielectric constant

Solvent	Self-solvated MEP value
Water	−40.2
DMSO	−53.7
Acetonitrile	−46.6
DMF	−51.9
Methanol	−37.5
Acetone	−43.9
Dichloromethane	−15.4
Trichloromethane	−8.4
Diethylether	−33.2

Regarding the chalcogen bond donors **3** and **4** (Fig. 2b), α = 0° and alpha = 90° correspond to the locations of the two σ-holes, moving within the molecular plane. In these cases, the MEP remains large and positive along the entire arc connecting both σ-holes. This indicates that the electrophilic region is less localized than in halogenated systems, suggesting that chalcogen bonds may exhibit lower directionality compared to halogen bonds.

To quantify the nucleophilicity of the media, the MEP minima ($V_{s,min}$) of the seven solvents were calculated in their self-solvated states. These values, provided in Table 2, serve as a metric for the competitive strength of the lone pairs of each solvent. Among the solvents studied, DMSO (−53.7 kcal mol^{-1}) and DMF (−51.9 kcal mol^{-1}) exhibit the most negative MEP values, indicating they are the most competitive nucleophiles for the σ-hole sites. Conversely, dichloromethane and chloroform are the least competitive solvents; their MEP values at the negative belts of the chlorine atoms are −15.4 and −8.4 kcal mol^{-1}, respectively, evidencing their poor ability to act as lone-pair donors.

Energetic analysis

The interaction energies (E_{int}) for the complexes of halogen bond donors **1** and **2** with the nine solvents are presented in Table 3. These values are similar to those reported in previous studies.[30,35] For instance, the complexes of **1** and **2** with dimethyl ether were

Table 3 Interaction energies (E_{int}, kcal mol^{-1}) in solvent and vacuo, HaB geometric features (distances in Å and angles in °), and electron density (ρ, a.u.) values for the complexes of **1** and **2** with the solvents

Complex	E_{int} (vacuo)	E_{int} (solvent)	Dist.	Angle	ρ
1·W	−3.1	−2.1	2.980	177.5	0.0130
1·DMSO	−5.2	−3.7	2.873	176.8	0.0161
1·ACN	−2.9	−1.7	3.120	180.0	0.0101
1·DMF	−4.2	−3.0	2.888	173.1	0.0158
1·MEOH	−3.5	−2.7	2.946	175.8	0.0143
1·ACE	−4.3	−3.3	2.969	178.0	0.0129
1·DCM	−2.5	−2.0	—	—	—
1·TCM	−2.5	−2.1	—	—	—
1·DEE	−4.3	−3.8	2.991	171.5	0.0133
2·W	−4.6	−3.6	2.976	178.0	0.0164
2·DMSO	−7.6	−5.9	2.832	178.4	0.0218
2·ACN	−4.3	−2.9	3.079	180.0	0.0140
2·DMF	−6.3	−5.0	2.853	175.5	0.0212
2·MEOH	−5.0	−4.3	2.932	177.5	0.0183
2·ACE	−5.9	−4.8	2.941	179.1	0.0173
2·DCM	−2.9	−2.1	3.640	162.9	0.0076
2·TCM	−2.6	−1.9	3.779	152.6	0.0061
2·DEE	−5.6	−5.1	3.014	173.3	0.0161

previously reported with values of −4.2 and −5.7 kcal mol^{-1}, almost identical to the complexes of DEE in Table 1.[70] A comparison between vacuum and solvent-phase calculations reveals a consistent reduction in the magnitude of E_{int} when the dielectric medium is accounted for. For instance, the interaction energy for the **2**·DMSO complex decreases from −7.6 kcal mol^{-1} *in vacuo* to −5.9 kcal mol^{-1} in the solvent phase. This attenuation is expected as the solvent medium stabilizes the isolated monomers, effectively competing with the formation of the noncovalent complex.

The interaction energies are consistently stronger for iodine (**2**) than for bromine (**1**) across all studied media with the exception of chloroform (TCM). It should be noted, however, that the **1**·DCM complex is not directly comparable to the **2**·DCM complex because no halogen bond is formed in the former, as detailed below. The stronger HaB energies for iodine (**2**) are in agreement with the MEP analysis, which showed more positive σ-hole values for the heavier, more polarizable iodine atom. Specifically, the interaction energy for **2** in DMSO is −5.9 kcal mol^{-1} compared to −3.7 kcal mol^{-1} for **1** in the same solvent.

This trend confirms that the increased electrophilicity of the iodine atom translates directly into a more robust halogen bond. In terms of absolute interaction energies in solution, the results provide a clear hierarchy of solvent competitiveness. The most negative (strongest) interaction energies are observed for DMSO (up to −5.9 kcal mol^{-1} for **2**) and DMF (−5.0 kcal mol^{-1} for **2**), identifying them as highly competitive media that may "poison" the electrophilic sites. Conversely, acetonitrile (−1.7 and −2.9 kcal mol^{-1}) and chloroform (−1.9 and −2.1 kcal mol^{-1}) show the weakest interactions in the solvent phase. Moreover, dichloromethane and water also exhibit weak interactions (ranging −2.0 to −3.6 kcal mol^{-1}). Consequently, from an experimental perspective, solvents like ACN, water, DCM and TCM appear more adequate for promoting halogen bonding (HaB) with external substrates, as they exhibit the lowest competitive binding to the σ-hole, setting aside potential solubility issues.

The structural and electronic descriptors of the HaB also provide insight into the interaction strength. In most cases, the HaB distances (d) and the electron density values (ρ) at the bond critical points (BCPs) correlate well with the interaction energies; shorter distances and higher ρ values generally correspond to stronger interactions. For example, the **2**·DMSO complex exhibits both the shortest distance (2.832 Å) and the highest electron density (0.0218 a.u.). However, in certain complexes, such as those involving diethylether (DEE) or acetone (ACE), the correlation between E_{int} and ρ is less direct. These discrepancies are likely due to the presence of secondary noncovalent contacts, such as those between the hydrogen atoms of the solvent and the negative belts of the halogen atoms. These additional interactions contribute to the total binding energy but are not fully captured by the ρ value at the primary HaB BCP. A detailed discussion of these supplementary contacts will be provided in the following section regarding the QTAIM analysis.

The interaction energies for the complexes involving chalcogen bond donors **3** and **4** with the nine solvents are summarized in Table 4. Similar to the halogen bonds, a significant reduction in interaction strength is observed when moving from vacuum to the solvent phase due to the stabilizing effect of the dielectric medium on the monomers. The results show that tellurium based donor **4** forms consistently stronger interactions than selenium based donor **3**. For example, the interaction of **4** with DMSO in the solvent phase is −7.6 kcal mol^{-1}, whereas for **3** it is −4.1 kcal mol^{-1}. This trend is entirely consistent with the MEP analysis, which identified **4** as having the most electrophilic σ-holes in the series. Regarding solvent competitiveness for chalcogen bonding sites, DMSO and DMF are the most competitive solvents, showing the strongest binding energies of −7.6 and −7.0 kcal mol^{-1} for **4**, respectively. Acetonitrile remains the least competitive organic solvent for compound **3**, with an interaction energy of −1.5 kcal mol^{-1}. For compound **4**, dichloromethane and chloroform are the least competitive (−2.8 and −2.7 kcal mol^{-1}, respectively), closely followed by acetonitrile (−3.1 kcal mol^{-1}), making them ideal candidates for experimental applications where donor availability is critical. Water also shows relatively low competitive binding, ranging from −2.3 to −4.7 kcal mol^{-1}, compared to the strong polar aprotic solvents. The distances and ρ values at the BCPs generally reflect the calculated energies. Complex **4**·DMSO, which has the strongest interaction, also exhibits the shortest distance of 2.724 Å and the highest electron density of 0.0256 a.u. As noted with the halogen bonds, cases where the energy does not perfectly correlate with the ρ value, such as with diethylether, suggest the presence of auxiliary interactions between the solvent and the CF_3 groups or the Se/Te lone pairs. These secondary contacts provide additional stabilization to the complex beyond the primary chalcogen bond.

When comparing the two types of noncovalent interactions, the chalcogen bonds generally exhibit higher interaction energies than the halogen bonds in the solvent phase. For example, the tellurium donor **4** reaches an interaction energy of −7.6 kcal mol^{-1} in DMSO, which is significantly more negative than the −5.9 kcal mol^{-1} observed for the iodine donor **2** in the same medium. This enhanced strength in chalcogen bonding

Table 4 Interaction energies (E_{int}, kcal mol^{-1}) in solvent and vacuo, ChB geometric features (distances in Å and angles in °) and electron density (ρ, a.u.) values for the complexes of **3** and **4** with the solvents

Complex	E_{int} (vacuo)	E_{int} (solvent)	Dist.	Angle	ρ
3·W	−4.0	−2.3	2.918	172.8	0.0156
3·DMSO	−6.6	−4.1	2.797	174.4	0.0187
3·ACN	−3.1	−1.5	3.227	174.3	0.0089
3·DMF	−5.3	−3.6	2.816	168.6	0.0195
3·MEOH	−4.1	−3.0	2.873	171.9	0.0174
3·ACE	−4.9	−3.5	3.024	176.3	0.0125
3·DCM	−3.0	−2.5	3.714	153.8	0.0060
3·TCM	−2.9	−2.5	3.773	166.7	0.0050
3·DEE	−5.2	−4.4	3.090	169.0	0.0112
4·W	−6.6	−4.7	2.883	165.6	0.0200
4·DMSO	−10.2	−7.6	2.724	170.2	0.0256
4·ACN	−5.5	−3.1	3.033	169.4	0.0155
4·DMF	−8.6	−7.0	2.741	166.6	0.0265
4·MEOH	−6.5	−5.4	2.852	165.8	0.0216
4·ACE	−7.6	−5.9	2.882	172.2	0.0199
4·DCM	−3.6	−2.8	3.713	161.8	0.0073
4·TCM	−3.3	−2.7	3.811	173.7	0.0056
4·DEE	−7.3	−6.5	2.985	168.3	0.0163

is consistent with the MEP analysis, as the presence of two electron-withdrawing trifluoromethyl groups in **4** creates a more electrophilic environment than the single substituent in the halogenated models. Furthermore, while both systems show a similar sensitivity to solvent competition, the tellurium and selenium donors maintain higher absolute binding energies across most organic media compared to their bromine and iodine counterparts. These results suggest that chalcogen bond donors may be more robust in polar environments, provided that a non-competitive solvent like acetonitrile is used to minimize site poisoning.

The geometric data summarized in Tables 3 and 4 further support the directionality differences identified in the MEP analysis if the very poor electron donor solvents DCM and TCM are not considered. The halogen bond angles (A) in Table 3 are significantly closer to linearity (ranging from 171.5° to 180.0°) compared to the chalcogen bond angles in Table 4 (ranging from 165.8° to 176.3°). This higher degree of linearity for halogen bonds aligns with the results shown in Fig. 2a, where the electrophilic potential drops sharply when moving away from the σ-hole axis. In contrast, the more pronounced deviations from linearity observed for the chalcogen bonds are consistent with the broader, less localized positive MEP regions shown in Fig. 2b, which allow for a wider range of favourable approach angles for the solvent nucleophiles.

It is important to note that while water appears to be a relatively poor competitive solvent for the electrophilic sites compared to strong polar aprotic solvents, these results must be interpreted with caution. The current model primarily evaluates the "poisoning" of the σ-hole donor by the solvent lone pairs. However, the protic nature of water allows it to effectively solvate the nucleophilic guest or substrate through hydrogen bonding. This competitive solvation of the nucleophile can significantly hinder the formation of halogen or chalcogen bonds in experimental settings, as the solvent would compete for both the electrophile and the nucleophile. Consequently, these interaction energies describe only the electrophilic component of the competitive binding process, and a complete experimental picture must also account for the competitive solvation of the nucleophilic species.

QTAIM study

The topological analysis of the electron density through the quantum theory of atoms in molecules (QTAIM) confirms the existence and nature of the noncovalent interactions. The distribution of bond critical points (BCPs), represented as fuchsia spheres, and the bond paths, indicated by dashed lines, are shown in Fig. 3. Because the complexes of compound **1** with DCM and TCM do not exhibit halogen bonds (HaBs) and instead only display hydrogen bonds (HBs), the HaB DCM and TCM complexes of **2** are included in Fig. 3 for comparison alongside the **1**·TCM complex, which serves as a representative example of these HBs. Since the distribution of BCPs and bond paths for the remaining solvents is identical across all complexes of **2**, only the bromine complexes are explicitly discussed here.

In most complexes, such as those with acetonitrile, water, methanol, and DMF, the QTAIM analysis reveals a single BCP

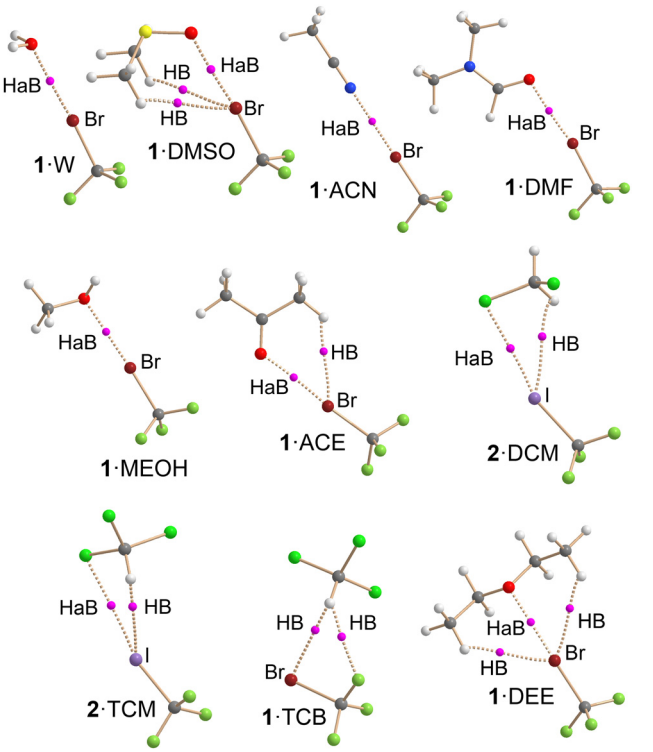

Fig. 3 QTAIM distribution of BCPss (fuchsia spheres) and bond paths (dashed bonds) for the complexes of compound **1** with the seven solvents studied. The topology for the complexes of **2** is identical. Primary halogen bonds (HaB) and auxiliary hydrogen bonds (HB) are indicated.

and bond path connecting the lone pair donor atom (nitrogen or oxygen) of the solvent to the electrophilic bromine atom. This confirms a straightforward halogen bonding (HaB) interaction. However, the complexes involving diethylether (**1**·DEE), acetone (**1**·ACE), and DMSO (**1**·DMSO) exhibit a more complex topological landscape. In these cases, additional bond paths and BCPs are observed, characterizing extra CH···Br hydrogen bonds between the hydrogen atoms of the solvent and the halogen atom. This also occurs in complexes **2**·DCM and **2**·TCM, where extra CH···I H-bonds assist the I···Cl HaBs.

These extra hydrogen bonds explain the energetic behaviour observed in the previous section. In these specific complexes, the total interaction energy is the result of both the primary HaB and these supplementary C–H···Br contacts. Consequently, this explains why the interaction energies for DEE, ACE, and DMSO were higher than what would be predicted solely by the electron density (ρ) at the primary HaB bond critical point. The presence of these auxiliary contacts provides additional stabilization that is not captured by looking at the HaB BCP in isolation, confirming that the total binding strength in these media is a multi-center phenomenon.

The topological analysis of the chalcogen bonded complexes reveals a diverse set of secondary interactions that complement the primary chalcogen bond (see Fig. 4). In the selenium complexes **3**, similar to the halogenated systems, diethylether, acetone, dichloromethane and DMSO exhibit additional hydrogen bonding contacts. However, specific structural differences

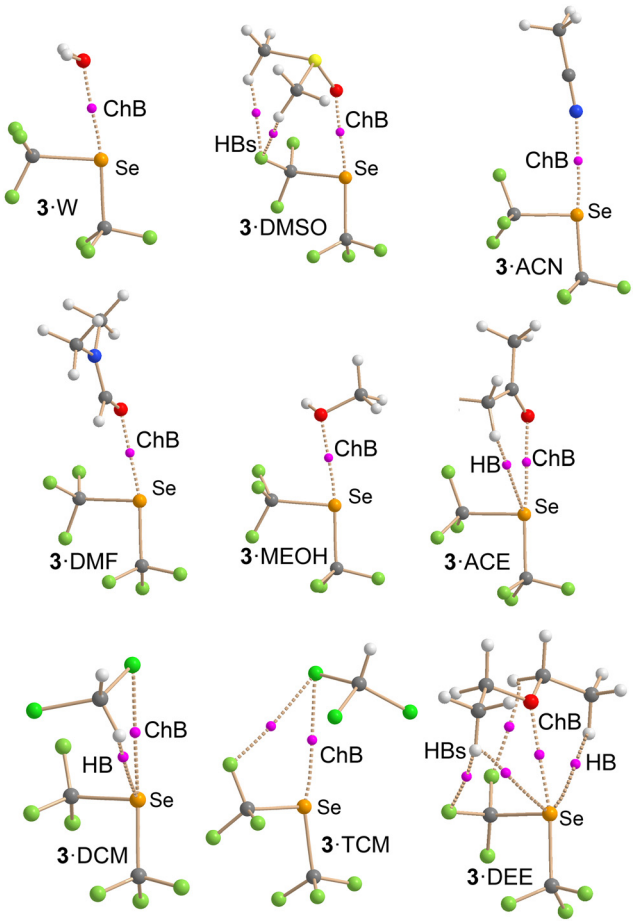

Fig. 4 QTAIM distribution of bond critical points (fuchsia spheres) and bond paths (dashed lines) for the complexes of compound **3** with the seven solvents. Primary chalcogen bonds and auxiliary hydrogen bonds are indicated.

emerge in the binding modes. In the **3** DMSO complex, the supplementary hydrogen bonds are directed exclusively toward the CF_3 groups, in **3**·DCM the HB is directed to the Se and the **3** DEE complex establishes a mixed network consisting of two C–H···F and two C–H···Se contacts. Finally, in the **3**·TCM and extra Cl···F contact is observed.

Distinct topological differences were also observed between the selenium **3** and tellurium **4** complexes specifically for the acetonitrile and DEE media (see Fig. 5). In the **4** ACN complex, the stabilization is enhanced by π-hole (C≡N)···F contacts rather than standard hydrogen bonds. For the **4** DEE complex, the interaction is characterized by a more extensive network of hydrogen bonds, involving four C–H···F and two C–H···Te contacts.

These findings provide a clear rationale for the energetic and electron density trends observed in Table 4. In complexes like **4** DMSO, the very high interaction energy of −7.6 kcal mol^{-1} correlates with a high ρ value of 0.0256 a.u. because the primary chalcogen bond is exceptionally strong. In the DEE complexes, the interaction energies of −4.4 kcal mol^{-1} for **3** and −6.5 kcal mol^{-1} for **4** appear disproportionately high compared to their respective ρ values at the BCP. This is explained by the multi center nature of

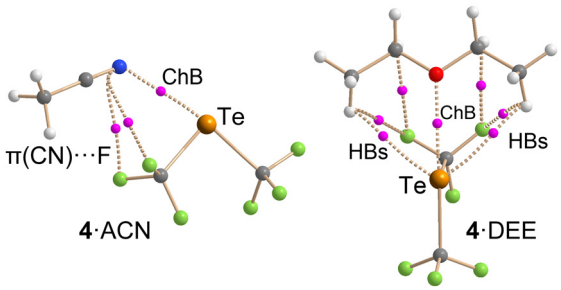

Fig. 5 Detailed QTAIM distribution for the complexes of **4** with ACN and DEE, highlighting the π-hole (CN)···F contacts and the extended network of hydrogen bonds.

the binding, where the total energy accounts for the primary chalcogen bond plus the significant contribution from the network of auxiliary C–H···F and C–H···Ch hydrogen bonds. Furthermore, the presence of π-hole (C≡N)···F contacts in the tellurium complex helps explain why acetonitrile shows a more significant interaction with the tellurium donor of −3.1 kcal mol^{-1} compared to the −1.5 kcal mol^{-1} observed for the selenium analogue. By accounting for these supplementary contacts, it becomes evident that the total interaction energy is a composite value, whereas the ρ at the bond critical point specifically measures the local strength of the primary σ-hole interaction.

Conclusions

In this work, we have provided a systematic classification of common laboratory solvents based on their competitiveness for electrophilic σ-hole sites in halogen and chalcogen bonding. Through a detailed DFT study, we analysed the interaction of nine solvents with four representative model molecules. The MEP analysis revealed that the utilization of a continuum model of the solvent has a small influence on the σ-hole potential, with values being more positive for the heavier elements tellurium and iodine. We observed that tellurium in compound **4** is more electrophilic than iodine in compound **2**, which is attributed to the presence of two electron-withdrawing substituents. Furthermore, the variation of the MEP as a function of the angle alpha suggested that halogen bonds involving bromine are more directional than those involving iodine, while chalcogen bonds appear less directional overall due to positive potentials extending between symmetric σ-holes.

The energetic analysis showed a consistent reduction of interaction energies in the solvent phase compared to vacuo. DMSO and DMF were identified as the most competitive solvents, exhibiting the strongest binding energies and the most negative MEP minima, which indicates a high potential for poisoning catalytic or receptor sites. Conversely, dichloromethane, chloroform, acetonitrile and water emerged as the least competitive media in terms of direct σ-hole occupancy. However, we noted that the protic nature of water necessitates careful consideration, as it may effectively solvate nucleophilic substrates. Furthermore, the practical use of water is often limited by the poor solubility in case of using neutral organic chalcogen donor receptors or catalysts.

QTAIM analysis shows that solvents like dichloromethane, chloroform, diethylether, acetone, and DMSO establish additional C–H···F, C–H···Br, or C–H···Se/Te hydrogen bonds, complementing the primary σ-hole interactions. In case of CH_3Br, dichloromethane and chloroform interact exclusively *via* H-bonds, evidencing a very poor nucleophilicity. These auxiliary contacts explain the lack of direct correlation between interaction energies and electron density at the primary BCP in certain cases. Our results provide a practical guide for experimentalists to identify the least competitive solvents, thereby optimizing the efficiency of halogen and chalcogen bonding driven molecular recognition and catalytic processes.

Author contributions

E. M. and M. R: formal analysis, investigation, methodology, software. A. F.: conceptualization, funding acquisition, visualization, validation, supervision, resources, project administration, writing – original draft and writing – review & editing.

Conflicts of interest

There are no conflicts to declare.

Data availability

The data that support the findings of this study are available in supporting information (SI) of this article. The rest of data is available directly from the manuscript. Supplementary informatlion (SI) available: Cartesian coordinates of all optimized compounds and Table S1. See DOI: https://doi.org/10.1039/d6cp01283c.

Acknowledgements

A. F. is grateful to project PID2023-148453NB-I00, Ministerio de Ciencia, Innovación y Universidades of Spain (MCIU/AEI/10.13039/501100011033) and the European Regional Development Fund (FEDER).

References

1 H.-J. Schneider, *J. Phys. Org. Chem.*, 2022, **35**, e4340.
2 H.-J. Schneider, *Chem. Soc. Rev.*, 1994, **23**, 227–234.
3 J. G. Dunitz and A. Gavezzotti, *Chem. Soc. Rev.*, 2009, **38**, 2622–2633.
4 R. S. Drago, *Structure and Bonding*, Springer, Berlin, 1973, p. 73.
5 H.-J. Schneider, *Angew. Chem., Int. Ed.*, 2009, **48**, 3924–3977.
6 F. Biedermann and H.-J. Schneider, *Chem. Rev.*, 2016, **116**, 5216–5300.
7 J. G. Dunitz and A. Gavezzotti, *Cryst. Growth Des.*, 2012, **12**, 5873–5877.
8 *Supramolecular Materials and Technologies, Perspectives in Supramolecular Chemistry*, ed. D. N. Reinhoudt, Wiley, 1999, vol. 4.
9 B. Gómez-González, N. Basílio, B. Vaz, M. R. Paleo, F. J. Sardina, M. Pérez-Lorenzo and L. García-Río, *J. Org. Chem.*, 2025, **90**, 6134–6145.
10 A. B. Grommet, J. Wang and R. Zhang, *et al.*, *Chem. Sci.*, 2024, **15**, 16480–16484.
11 V. Sehgal, S. P. Pandey and P. K. Singh, *Carbohydr. Polym.*, 2024, **323**, 121348.
12 H. Yin, Q. Cheng, D. Bardelang and R. Wang, *JACS Au*, 2023, **3**, 2356–2377.
13 Y.-C. Pan, X.-Y. Hu and D.-S. Guo, *Angew. Chem., Int. Ed.*, 2021, **60**, 2768–2794.
14 H. Zhu, Q. Li, L. E. Khalil-Cruz, N. M. Khashab, G. Yu and F. Huang, *Sci. China: Chem.*, 2021, **64**, 688–700.
15 X. Li, M. Shen, J. Yang, L. Liu and Y.-W. Yang, *Adv. Mater.*, 2024, **36**, 2313317.
16 H.-J. Schneider, *Acc. Chem. Res.*, 2015, **48**, 1815–1822.
17 J. Cerny and P. Hobza, *Phys. Chem. Chem. Phys.*, 2007, **9**, 5291–5303.
18 L.-A. Gravillier and S. L. Cockroft, *Acc. Chem. Res.*, 2023, **56**, 3535–3544.
19 K. I. Assaf and W. M. Nau, *Acc. Chem. Res.*, 2023, **56**, 3451–3461.
20 C. A. Hunter, *Angew. Chem., Int. Ed.*, 2004, **43**, 5310–5324.
21 K. D. Shimizu, *Nat. Chem.*, 2013, **5**, 989–990.
22 C. A. Hunter, *Chem. Sci.*, 2013, **4**, 834–848.
23 J. Hwang, B. E. Dial, P. Li, M. E. Kozik, M. D. Smith and K. D. Shimizu, *Chem. Sci.*, 2015, **6**, 4358–4364.
24 C. Bravin, J. A. Piekos, G. Licini, C. A. Hunter and C. Zonta, *Angew. Chem., Int. Ed.*, 2021, **60**, 23871–23877.
25 H. Liu and K. D. Shimizu, *Acc. Chem. Res.*, 2023, **56**, 3572–3580.
26 T. Clark, M. Hennemann, J. S. Murray and P. Politzer, *J. Mol. Model.*, 2007, **13**, 291–296.
27 A. Bauzá, T. J. Mooibroek and A. Frontera, *ChemPhysChem*, 2015, **16**, 2496–2517.
28 P. Politzer and J. S. Murray, *Crystals*, 2017, **7**, 212.
29 P. Politzer, J. S. Murray and M. C. Concha, *J. Mol. Model.*, 2008, **14**, 659–665.
30 P. Politzer, J. S. Murray and T. Clark, *Phys. Chem. Chem. Phys.*, 2013, **15**, 11178–11189.
31 P. Politzer, J. S. Murray and T. Clark, *Top. Curr. Chem.*, 2015, **358**, 19–42.
32 P. Politzer, J. S. Murray and T. Clark, *Phys. Chem. Chem. Phys.*, 2021, **23**, 16458–16468.
33 P. Politzer and J. S. Murray, *J. Comput. Chem.*, 2018, **39**, 464–471.
34 A. Bauzá, R. Ramis and A. Frontera, *J. Phys. Chem. A*, 2014, **118**, 2827–2834.
35 P. Politzer and J. S. Murray, *ChemPhysChem*, 2020, **21**, 579–588.
36 P. Politzer and J. S. Murray, *Crystals*, 2019, **9**, 165.
37 G. Cavallo, P. Metrangolo, R. Milani, T. Pilati, A. Priimagi, G. Resnati and G. Terraneo, *Chem. Rev.*, 2016, **116**, 2478–2601.
38 G. R. Desiraju, P. S. Ho, L. Kloo, A. C. Legon, R. Marquardt, P. Metrangolo, P. Politzer, G. Resnati and K. Rissanen, *Pure Appl. Chem.*, 2013, **85**, 1711–1713.
39 P. Scilabra, G. Terraneo and G. Resnati, *Acc. Chem. Res.*, 2019, **52**, 1313–1324.
40 C. B. Aakeroy, D. L. Bryce, G. R. Desiraju, A. Frontera, A. C. Legon, F. Nicotra, K. Rissanen, S. Scheiner, G. Terraneo,

P. Metrangolo and G. Resnati, *Pure Appl. Chem.*, 2019, **91**, 1889–1892.
41 Y. Li, C. Zhao, Z. Wang and Y. Zeng, *J. Phys. Chem. A*, 2024, **128**(3), 507–527.
42 C. C. Robertson, J. S. Wright, E. J. Carrington, R. N. Perutz, C. A. Hunter and L. Brammer, *Chem. Sci.*, 2017, **8**, 5392–5398.
43 A. E. Settle, L. Berstis, S. Zhang, N. A. Rorrer, H. Hu, R. M. Richards, G. T. Beckham, M. F. Crowley and D. R. Vardon, *ChemSusChem*, 2018, **11**, 1768–1780.
44 A. Yoshimura and V. V. Zhdankin, *Chem. Rev.*, 2016, **116**, 3328–3435.
45 R. L. Sutar, E. Engelage, R. Stoll and S. M. Huber, *Angew. Chem., Int. Ed.*, 2020, **59**, 6806–6810.
46 S. Portela, J. J. Cabrera-Trujillo and I. Fernandez, *J. Org. Chem.*, 2021, **86**, 5317–5326.
47 C. Xu, V. U. B. Rao, J. Weigen and C. C. J. Loh, *Nat. Commun.*, 2020, **11**, 4911.
48 S. M. Walter, F. Kniep, E. Herdtweck and S. M. Huber, *Angew. Chem., Int. Ed.*, 2011, **50**, 7187–7191.
49 F. Kniep, L. Rout, S. M. Walter, H. K. Bensch, S. H. Jungbauer, E. Herdtweck and S. M. Huber, *Chem. Commun.*, 2012, **48**, 9299–9301.
50 F. Kniep, S. M. Walter, E. Herdtweck and S. M. Huber, *Chem. – Eur. J.*, 2012, **18**, 1306–1310.
51 E. Engelage, H. Hijazi, M. Gartmann, L. M. Chamoreau, B. Schollhorn, S. M. Huber and C. Fave, *Phys. Chem. Chem. Phys.*, 2021, **23**, 4344–4352.
52 G. Sekar, V. V. Naira and J. Zhu, *Chem. Soc. Rev.*, 2024, **53**, 586–605.
53 S. Benz, J. López-Andarias, J. Mareda, N. Sakai and S. Matile, *Angew. Chem., Int. Ed.*, 2017, **56**, 812–815.
54 P. Wonner, L. Vogel, M. Düser, L. Gomes, F. Kniep, B. Mallick, D. B. Werz and S. M. Huber, *Angew. Chem., Int. Ed.*, 2017, **56**, 12009–12012.
55 P. Wonner, L. Vogel, F. Kniep and S. M. Huber, *Chem. – Eur. J.*, 2017, **23**, 16972–16975.
56 S. Benz, J. Mareda, C. Besnard, N. Sakai and S. Matile, *Chem. Sci.*, 2017, **8**, 8164–8169.
57 P. Wonner, A. Dreger, L. Vogel, E. Engelage and S. M. Huber, *Angew. Chem., Int. Ed.*, 2019, **58**, 16923–16927.
58 P. Wonner, T. Steinke, L. Vogel and S. M. Huber, *Chem. – Eur. J.*, 2020, **26**, 1258–1262.
59 W. Wang, H. Zhu, S. Liu, Z. Zhao, L. Zhang, J. Hao and Y. Wang, *J. Am. Chem. Soc.*, 2019, **141**, 9175–9179.
60 W. Wang, H. Zhu, L. Feng, Q. Yu, J. Hao, R. Zhu and Y. Wang, *J. Am. Chem. Soc.*, 2020, **142**, 3117–3124.
61 H. Y. Duan, S. T. Han, T. G. Zhan, L. J. Liu and K. D. Zhang, *Angew. Chem., Int. Ed.*, 2023, **5**, e202212707.
62 C. C. Robertson, R. N. Perutz, L. Brammer and C. A. Hunter, *Chem. Sci.*, 2014, **5**, 4179–4183.
63 M. J. Frisch, G. W. Trucks, H. B. Schlegel, G. E. Scuseria, M. A. Robb, J. R. Cheeseman, G. Scalmani, V. Barone, G. A. Petersson, H. Nakatsuji *et al.*, *Gaussian 16, Revision C.01*, Gaussian, Inc., Wallingford, CT, 2016.
64 C. Adamo and V. Barone, *J. Chem. Phys.*, 1999, **110**, 6158.
65 S. Grimme, J. Antony, S. Ehrlich and H. Krieg, *J. Chem. Phys.*, 2010, **132**, 154104.
66 F. Weigend and R. Ahlrichs, *Phys. Chem. Chem. Phys.*, 2005, **7**, 3297–3305.
67 J. Tomasi, B. Mennucci and R. Cammi, *Chem. Rev.*, 2005, **105**, 2999–3093.
68 R. F. W. Bader, *Atoms in Molecules: A Quantum Theory*, Oxford University Press, Oxford, 1990.
69 T. A. Keith, *AIMAll, Version 19.10.12*, TK Gristmill Software, Overland Park, KS, 2019.
70 B. Pinter, N. Nagels, W. A. Herrebout and F. de Proft, *Chem. – Eur. J.*, 2013, **19**, 519–530.